The 2015 World Congress on
Aeronautics, Nano, Bio, Robotics, and Energy (ANBRE15)
Incheon, Korea, August 25-28, 2015

Invited Paper

Progress and Challenge of Limiting Strategy for Higher-Order CFD Methods

*Chongam Kim[1)]

[1)] *Department of Aerospace Engineering, Seoul National University, Seoul 151-744, Korea*
[1)] *chongam@snu.ac.kr*

ABSTRACT

This paper presents the recent progress of multi-dimensional limiting process (MLP) and discuss some issues for further improvements. MLP, which has been originally developed in finite volume method (FVM), provides an accurate, robust and efficient oscillation-control mechanism in multiple dimensions for linear reconstruction. This limiting philosophy can be hierarchically extended into higher-order *Pn* approximation/reconstruction. The resulting algorithm, called the hierarchical MLP, facilitates the capturing of detailed flow structures while maintaining the formal order-of-accuracy in smooth region and providing accurate non-oscillatory solutions across discontinuous region. This algorithm has been originally developed within the modal DG framework and extended into a nodal framework, most notably the FR/CPR framework. Troubled-cells are detected by applying the MLP condition and smooth extrema detector. The final accuracy is then determined by the projection procedure and the hierarchical MLP limiting step. Through extensive numerical analyses and computations ranging from scalar conservation laws to fluid systems, it is observed that the proposed limiting approach yields the outstanding performances in capturing compressible inviscid and viscous flow features. Some challenging issues are also mentioned to improve and extend the current approach for higher-order simulations of high-Reynolds number compressible flows.

1. INTRODUCTION

Up to now, second-order accurate computational fluid dynamics (CFD) methods with some discontinuity-capturing strategy are widely used to analyze compressible viscous flows. Theoretically, these approaches guarantee the minimal accuracy to recover essential physics of high-Reynolds number compressible flows. Indeed, they have witnessed remarkable successes in many classes of engineering and scientific applications. At the same time, however, they also unveil some limitations, particularly

[1)] Professor

in capturing unsteady vortex-dominated flow structures due to excessive numerical diffusion. From this perspective, higher-order methods are convincing alternatives in the sense that they can provide the detailed flow structures by upgrading the accuracy of spatial and temporal discretization with reasonable computational resources (Cockburn 2000, Wang 2007, Vincent and Jameson 2011, Wang 2011).

During the past few decades, various higher-order discretization methods have been developed. In order to handle complex geometry, these methods usually combine the merits of both finite volume methods (FVM) and finite element methods (FEM), which makes it possible to develop higher-order approximation/reconstruction for each cell with a minimal stencil. Discontinuous Galerkin (DG) method is one of the widely-used and well-developed higher-order methods in hyperbolic conservation laws. Strong mathematical background and numerical analysis support it though overall formulations are relatively complex and expensive compared to FVM. Recently, Huynh proposed the flux reconstruction (FR) procedure (Huynh 2007, Huynh 2009), which provides a unifying framework of many higher-order methods. In addition, Wang introduced a lifting collocation operator (Wang 2009) to deal with multi-dimensional problems on simplex and mixed grids. The two approaches were combined and renamed as correction procedure via reconstruction (CPR), which possesses many merits of higher-order methods in terms of accuracy and stability, while it is more simple and efficient. Recent studies also show some encouraging results in capturing compressible flow features (Wang 2011). Furthermore, the energy stability of FR was rigorously studied by Vincent *et al.*, and as a result, energy stable flux reconstruction (ESFR) was developed (Vincent *et al.* 2011, Castonguay 2011).

At the same time, a few obstacles have surfaced in extending higher-order CFD methods, including CPR, into high speed unsteady flows. One of them is to design a robust and efficient oscillation-control algorithm to suppress unwanted oscillations around discontinuities without compromising the higher-order nature in smooth region. The main reason for such oscillations is the lack of providing a proper diffusion mechanism. Especially, the diminished numerical viscosity triggers multi-dimensional oscillations more often, and thus the study on the robust, accurate and efficient shock-capturing philosophy for multi-dimensional flows has become one of the essential issues in higher-order CFD methods.

Recently, the multi-dimensional limiting process (MLP) has been successfully proposed in the FVM framework. Compared with traditional limiting strategies, such as the TVD or ENO-type limiting, the MLP limiting can efficiently control unwanted oscillations particularly in multi-dimensional flow situations. By imposing the MLP condition on both cell-averaged and cell-vertex values, the MLP limiting can efficiently follow the multi-dimensional flow physics. A series of previous researches (Kim 2005, Yoon 2008, Park 2010, Park 2012) demonstrated that the MLP limiting possesses superior characteristics in terms of accuracy, robustness and efficiency in inviscid and viscous computations on structured and unstructured grids within the FVM framework. Since the proposed limiting algorithm relies only on the MLP stencil regardless of the order of approximation, it facilitates an easy extension to popular higher-order methods, such as DG method. As a way to stabilize the higher-order DG method, the original MLP condition is modified to take into account the behavior of local extrema produced by a cell-wise higher-order approximation. As a consequence, the augmented MLP

condition and the MLP-based troubled-cell marker are obtained, which pave the way to obtain the hierarchical DG-MLP formulation (Park 2014 (C&F)). By examining the numerical Gibbs' phenomenon caused by the sub-cell distribution and its propagation, the *P1*-projected MLP condition is newly obtained and applied to CPR method within the hierarchical DG-MLP formulation (Park submitted).

In this study, we present the progress of the MLP limiting strategy for higher-order schemes and discuss some issues to treat high-Reynolds number flows around realistic configurations. The paper is organized as follows. First, the hierarchical MLP limiting with the augmented MLP condition and *P1*-projected MLP condition is described in Section 2. In Section 3, extensive numerical experiments are carried out to assess the performance of the proposed limiting strategy for inviscid and viscous compressible flows involving shocks. Issues for further improvements are discussed in Section 4. Finally, conclusions are given in Section 5.

2. HIGHER-ORDER MULTI-DIMENSIONAL LIMITING STRATEGY

As well as stable time integration methods, an oscillation-control mechanism is essential to resolve compressible flows, especially the flows involved with shock waves. Limiting should be activated only on the troubled-cells to maintain higher-order accuracy across smooth extrema. An accurate troubled-cell marker, followed by a sophisticated limiting, is thus crucial to obtain an accurate monotone profile in the higher-order approximation. Some troubled-cell markers, such as the TVB marker (Cockburn 1998) or KXRCF marker (Krivodonova 2004), have been developed and combined with slope limiters or WENO-type limiters, but the accurate detection of the troubled-cells is not an easy task. Keeping this in mind, we establish the hierarchical MLP limiting strategy for the higher-order CFD methods to detect the troubled-cells. At first, we briefly summarize the MLP-u slope limiters and propose two troubled-cell detecting conditions: the augmented MLP condition and the newly developed *P1*-projected MLP condition. By combining one of the two conditions with the MLP-based smooth extrema detector, we describes the implementation of the hierarchical MLP limiting algorithm.

2.1 MLP-u Slope Limiter

In order to enforce the multi-dimensional monotonicity, the MLP condition has been proposed in the finite volume framework. This condition is simply an extension of the one-dimensional monotonicity condition by considering the case where the direction of local flow gradient is not aligned to the local grid line. The starting point of the MLP condition is that local extrema always occur at vertex point when sub-cell distribution is linear. This observation manifests that, i) treatment of vertex point is essential in limiting stage, ii) all information around vertex point should be incorporated to avoid multi-dimensional oscillations. As a result, we have the following MLP condition.

$$\bar{q}_{v_i}^{\min} \le q_j^{h,Pn}(\mathbf{x}) \le \bar{q}_{v_i}^{\max} \tag{1}$$

Here, q is the state variable, and $q_j^{h,Pn}$ is the sub-cell distribution obtained by a *Pn* approximation on the target cell T_j. $\bar{q}_{v_i}^{\min}, \bar{q}_{v_i}^{\max}$ are the minimum and maximum cell-averaged values among all neighboring cells that share any vertex, edge or face of T_j.

$$\bar{q}_{v_i}^{\min} = \min_{T_k \in S_{v_i}}(\bar{q}_k), \quad \bar{q}_{v_i}^{\max} = \max_{T_k \in S_{v_i}}(\bar{q}_k). \tag{2}$$

$$S_{v_i} = \{T_k \mid v_i \in T_k \text{ for some } v_i \in T_j\}, \quad S_{T_j} = \{T_k \mid v_i \in T_k \text{ for all } v_i \in T_j\} \tag{3}$$

In other words, S_{v_i} is the union of computational cells sharing the vertex v_i and S_{T_j} is the union of computational cells sharing any vertex of the cell T_j. S_{T_j} is called the MLP stencil (Park 2010, Park 2012). It is noted that the MLP condition can be applied to any type of mesh since it does not assume particular mesh connectivity. At the same time, it is also observed that well-controlled vertex value at interpolation/limiting stage makes it possible to produce a monotonic distribution of cell-averaged values. Extensive numerical experiments (Kim 2005, Yoon 2008, Park 2010, Park 2012) strongly support that the full realization of Eq. (1) is quite effective to preserve accurate monotone profiles.

This philosophy can be readily extended on unstructured grids with second-order accurate reconstruction. Sub-cell interpolation may start from the unstructured version of the MUSCL-type linear reconstruction as follows.

$$L[q_j^{h,P1}(\mathbf{x})] = \bar{q}_j + \phi_j P1_j(\mathbf{x}). \tag{4}$$

Here, ϕ_j is a slope limiter and $L[q_j^{h,P1}(\mathbf{x})]$ indicates the limited linear distribution. $L[q_j^{h,P1}(\mathbf{x})] = q_j^{h,P1}(\mathbf{x})$ when $\phi_j = 1$. For finite volume method,

$$P1_j(\mathbf{x}) = \nabla \bar{q}_j \cdot (\mathbf{x} - \bar{\mathbf{x}}_j), \tag{5}$$

where q is the state variable and $\nabla \bar{q}_j$ is the gradient on T_j. $\mathbf{x}$ is the position vector and $\bar{\mathbf{x}}_j$ is the centroid of the cell T_j. By applying the MLP condition to each vertex v_i of T_j (Eq. (1) and Eq. (2)), we can obtain the following range of MLP-u slope limiters.

$$0 \le \phi_j \le \min_{\forall v_i \in T_j} \left[\max \left(\frac{\bar{q}_{v_i}^{\min} - \bar{q}_j}{P1_j(\mathbf{x}_{v_i})}, \frac{\bar{q}_{v_i}^{\max} - \bar{q}_j}{P1_j(\mathbf{x}_{v_i})} \right) \right]. \tag{6}$$

From Eq. (6), MLP-u slope limiters can be formulated as follows.

$$\phi_{MLP} = \min_{\forall v_i \in T_j} \begin{cases} \Phi(r_{v_i,j}) & \text{if } \left| P1_j(x_{v_i}) \right| \ge \varepsilon_{\text{machine}} \\ 1 & \text{otherwise} \end{cases}, \tag{7}$$

$$r_{v_i,j} = \max\left(\frac{\overline{q}_{v_i}^{\min} - \overline{q}_j}{P1_j(\mathbf{x}_{v_i})}, \frac{\overline{q}_{v_i}^{\max} - \overline{q}_j}{P1_j(\mathbf{x}_{v_i})}\right), \tag{8}$$

$$0 \le \Phi(r) \le \min(1, r), \tag{9}$$

where $\varepsilon_{\text{machine}}$ is the machine epsilon. By determining $\Phi(r)$ to satisfy the maximum principle, we have the MLP-u1 and MLP-u2 limiters. Detailed implementation in unsteady and steady flows can be found in Park(2010) and Park(2012).

The stability characteristics of the MLP limiting is supported by the maximum principle. For multi-dimensional scalar conservation law, the MLP limiting under linear reconstruction guarantees the local maximum principle under a suitable CFL condition (Park 2010, Park 2012). It simply states that the updated solution at every time step by the MLP limiting satisfies the maximum principle both on cell-averaged and cell-vertex values, though the stencil involved is a bit different. Thus, the MLP limiting satisfies the LED condition in a truly multi-dimensional way (Park 2012). The MLP condition on the MLP stencil makes it realizable to capture multi-dimensional flow physics accurately while maintaining the second-order accuracy in smooth region.

2.2 Augmented MLP Condition

Equation (1) were used to identify and control the maximum-principle-violating cells in second-order finite volume methods. (Park 2010, Park 2012) For higher-order approximation greater than P1 polynomial, an additional condition is essential because local extrema no longer appear at a vertex point in *P1* approximation.

If we assume a discontinuity near the vertex point v_i, as shown in Fig. 1, higher-order *Pn* approximation would trigger unwanted oscillations in the blue-shaded region. For *P1* approximation, sub-cell value at any quadrature point in T_j can be readily controlled by limiting the vertex value at which local extrema always appear. For greater than *P1* approximation, we may have a quadrature point at which sub-cell value does lie outside the range imposed by the MLP condition (Eq. (1)), and thus the maximum principle can be violated. This may occur even if the vertex value does satisfy the MLP condition. Therefore, the MLP condition imposed on a single cell T_j is not complete enough to handle higher-order distribution, and it may allow spurious oscillations for the situation depicted in Fig. 1. As a remedy, we require all the approximated vertex values of S_{v_i} to satisfy the MLP condition since all $T_k \in S_{v_i}$ will be eventually influenced by the presence of the discontinuity through the dynamic exchange of the cell-interface flexes. In other words, when we check whether T_j is a troubled cell or not, we impose the MLP condition on S_{v_i} not just on T_j. From this perspective, we impose a stricter constraint than the MLP condition. The augmented MLP condition is then used as the MLP-based troubled-cell marker for higher-order approximation.

$$\overline{q}_{v_i}^{\min} \le \min_{T_k \in S_{v_i}}\left(q_k^{h,Pn}(\mathbf{x}_{v_i})\right), \max_{T_k \in S_{v_i}}\left(q_k^{h,Pn}(\mathbf{x}_{v_i})\right) \le \overline{q}_{v_i}^{\min}. \tag{10}$$

Here, $q_j^{h,Pn}(\mathbf{x}_{v_i})$ indicates the value at vertex v_i obtained from *Pn* approximation on $T_k \in S_{v_i}$. If any $q_j^{h,Pn}(\mathbf{x}_{v_i})$ violates Eq. (1), T_j is tagged as a troubled cell. Numerical experiments strongly support that the MLP slope limiter with the A-MLP condition is quite successful in handling multi-dimensional oscillations (Park 2014).

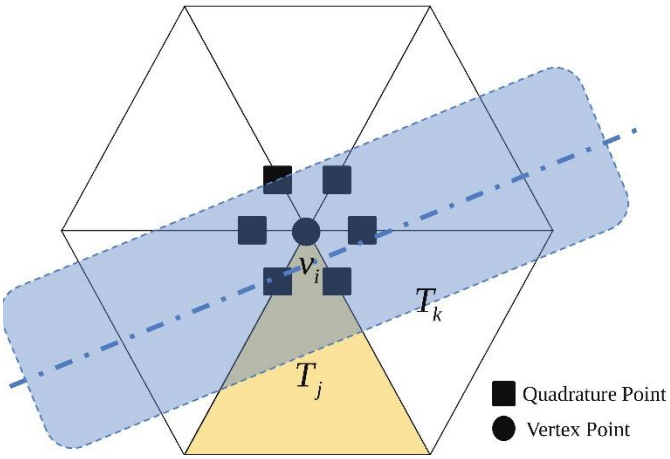

Figure 1: Discontinuity on the MLP stencil. (Dash-dot line is a discontinuity and spurious oscillations may occur in the blue-shaded region.)

2.3 P1-projected MLP Condition

While the augmented MLP condition is successful in detecting multi-dimensional discontinuous profile for higher-order methods, its performance to distinguish normal cells can be further improved. A MLP-based troubled-cell marker is newly proposed by examining the sub-cell distribution of the numerical Gibbs phenomenon. For the purpose of convenience, the analysis is performed using the modal DG method, but its consequence is equally valid to the CPR method.

In order to analyze the numerical behavior across discontinuous profiles, we consider the one-dimensional scalar conservation law with a simple square wave as an initial condition. After a few iterations, sub-cell distributions readily notes that oscillations have already developed in the higher-order modes and they are propagating into the cell-averaged values, though the cell-averaged values still maintain a monotonic profile. When oscillations in the higher-order modes are triggered, the *P1*-projected approximation acts as a precursor to warn non-monotone distributions by developing a steep gradient. From this observation, it is obtained that, i) oscillations are hierarchically propagating from the higher-order modes into the cell-averaged value, ii) oscillations strongly affect the *P1*-projected term to produce a monotonicity-violating steep gradient. This indicates that examining the monotonicity of the *P1*-projected term is enough to detect oscillations in the higher-order modes. Thus, we newly propose a simple and efficient limiting condition for higher-order approximations as follows.

$$\min(\bar{q}_i, \bar{q}_{i+1}) \le \Pi^1 q_j^{h,Pn}(\mathbf{x}_{v_i}) \le \max(\bar{q}_i, \bar{q}_{i+1}) \tag{11}$$

It is noted that this condition limits the linear term, and thus it can be readily extended into multiple dimensions by embracing the MLP philosophy on vertex point, leading to the following *P1*-projected MLP condition.

$$\bar{q}_{v_i}^{\min} \le \Pi^1 q_j^{h,Pn}(x_{v_i}) \le \bar{q}_{v_i}^{\max} \tag{12}$$

2.4 MLP Extrema Detector

The augmented MLP and *P1*-projected MLP conditions in themselves do not provide any mechanism to distinguish local smooth extrema. In order to preserve the accuracy across smooth extrema, we introduce a MLP extrema detector by examining the behavior of local extrema around the vertex v_i of the cell T_j.

First, we decompose the *Pn* approximation into the cell-average part, the linear part (*Pn*-projected slope) and the higher-order part (*P1*-filtered *Pn*) as follows:

$$q_j^{h,Pn}(\mathbf{x}_{v_i}) = \bar{q}_j + \underbrace{(\Upsilon(\mathbf{x}_{v_i}) - \bar{q}_j)}_{\text{Pn-projected slope}} + \underbrace{(q_j^{h,Pn}(\mathbf{x}_{v_i}) - \Upsilon(\mathbf{x}_{v_i}))}_{\text{P1-filtered Pn}} \tag{13}$$

$$\Upsilon(\mathbf{x}_{v_i}) = \Pi^1 q_j^{h,Pn}(\mathbf{x}_{v_i}) \tag{14}$$

The starting point is that the *Pn*-projected slope can be interpreted as the average slope of the *Pn* approximation. Then, from the mean value theorem, if local extrema appear in a small neighborhood of the vertex v_i, the gradient direction of $q_j^{h,Pn}(\mathbf{x}_{v_i})$ could be quite different from the direction of the *Pn*-projected slope. If one goes up, the other would go down. Even if they show the same trend, the magnitude of the gradient of $q_j^{h,Pn}(\mathbf{x}_{v_i})$ would be smaller than that of the *Pn*-projected slope. From this observation, we can readily deduce the following condition to detect smooth extrema near the vertex v_i.

- 1. If there is a local maximum near the vertex v_i,
  Pn-projected slope > 0, *P*1-filtered *Pn* < 0, and $q_j^{h,Pn}(\mathbf{x}_{v_i}) > \bar{q}_{v_i}^{\min}$.
- 2. If there is a local minimum near the vertex v_i,
  Pn-projected slope < 0, *P*1-filtered *Pn* > 0, and $q_j^{h,Pn}(\mathbf{x}_{v_i}) < \bar{q}_{v_i}^{\max}$.

(15)

The last inequalities ($q_j^{h,Pn}(\mathbf{x}_{v_i}) > \bar{q}_{v_i}^{\min}$, $q_j^{h,Pn}(\mathbf{x}_{v_i}) < \bar{q}_{v_i}^{\max}$) are necessary to treat a stiff gradient which may include physical discontinuities. Finally, in order to deal with a nearly constant region particularly when local grids become very coarse, we add the following deactivation threshold.

$$\left| q_j^{h,Pn}(x_{v_i}) - \bar{q}_j \right| \le \max\left(\varepsilon \times \left| \bar{q}_j \right|, \left| T_j \right| \right) \tag{16}$$

where ε is a small number to distinguish a constant region with machine error, 1×10^{-3} is a reasonable choice. $|T_j|$ is the area/volume of the cell T_j. Most of the extrema are well recognized by the condition $\square 1$ and $\square 2$, and only a very few cells are detected by Eq. (16).

2.5 Hierarchical MLP Limiting Algorithm

By combining the A-MLP or *P1*-projected MLP condition (Eq. (10) or Eq. (12)) and the extrema detector (Eq. (15) with Eq. (16)), we formulate the hierarchical MLP limiting strategy for arbitrary *Pn* approximation. $q_j^{h,Pn}(\mathbf{x})$ is firstly expressed in terms of Pm_j modes $(1\le m\le n)$ using the projection operator.

$$q_j^{h,Pn}(\mathbf{x}) = \bar{q}_j + P1_j(\mathbf{x}) + P2_j(\mathbf{x}) + ... + Pn_j(\mathbf{x}), \tag{17}$$

$$Pm_j(\mathbf{x}) = \Pi^m q_j^{h,Pn}(\mathbf{x}) - \Pi^{m-1} q_j^{h,Pn}(\mathbf{x}), \tag{18}$$

where Π^m indicates a projection operator to *Pm* space. The limiting procedure is then hierarchically carried out from the highest mode to the lowest $P1_j$ mode as follows.

$$\begin{aligned} L\left[q_j^{h,Pn}(\mathbf{x})\right] = \bar{q}_j + \phi_{MLP}\left(P1_j(\mathbf{x})\right) \\ + \varphi_j^{P2}(P2_j(\mathbf{x}) + \varphi_j^{P3}(P3_j(\mathbf{x}) + \varphi_j^{P4}(... + \varphi_j^{Pn} Pn_j(\mathbf{x})))). \end{aligned} \tag{19}$$

φ_j^{Pm} is the hierarchical MLP troubled-cell marker applied to the Pm_j mode of the cell T_j as follows.

$$\varphi_j^{Pm} = \min_{\forall v_i \in T_j} (\psi_{v_i,j}^{Pm}). \tag{20}$$

Depending on the choice of φ_j^{Pm}, we can propose two versions for the hierarchical MLP limiting.

• Hierarchical MLP limiting with the A-MLP condition and smooth extrema detector:

$$\psi_{v_i,j}^{Pm} = \begin{cases} 1 & \text{if Eq. (10) or Eq. (15) with Eq. (16) is satisfied,} \\ 0 & \text{else.} \end{cases} \tag{21}$$

• Hierarchical MLP limiting with the *P1*-projected MLP condition and smooth extrema detector:

$$\psi_{v_i,j}^{Pm} = \begin{cases} 1 & \text{if Eq. (12) or Eq. (15) with Eq. (16) is satisfied,} \\ 0 & \text{else.} \end{cases} \tag{22}$$

The MLP limiting procedure in Eq. (19) is applied in a hierarchical manner from the highest Pn_j mode to the lowest $P1_j$ mode, and the implementation procedure can be summarized as follows:

1. Apply the augmented MLP or *P1*-projected MLP condition (Eq. (10) or Eq. (12)) to the *Pn* approximated solution at every vertex v_i of the cell T_j.

2. Compute the hierarchical troubled-cell marker φ_j^{Pn} (Eq. (20)).

3. If the cell T_j is tagged as a normal cell (or $\varphi_j^{Pn}=1$), the highest order term is kept unlimited and the limiting procedure is completed. Otherwise ($\varphi_j^{Pn}=0$),

(a) if $n>2$, project the entire polynomial approximation onto V^{n-1} space and obtain $P(n-1)_j(\mathbf{x})$. And, repeat Step 1 for *P(n-1)* approximation.

(b) if $n=2$, project the entire polynomial approximation onto V^1 space. $P1_j(\mathbf{x})$ is limited by the MLP-u slope limiters (Eq. (7)).

In modal DG with orthogonal basis functions, the projection procedure is realized by simply truncating the higher-order Pn_j mode. In case of nodal formulation, such as CPR, the projection procedure is carried out by obtaining $q_j^{h,Pm}(x)=\sum_l \tilde{q}_{l,j}^{h,Pm} L_{l,j}^{Pm}(\mathbf{x})$ $(m<n)$ from the *Pn* approximation as follows.

$$\sum_l \left(\int_{T_j} L_{l,j}^{Pm}(\mathbf{x}) L_{k,j}^{Pm}(\mathbf{x}) dV \right) \tilde{q}_{l,j}^{h,Pm} = \int_{T_j} q_j^{h,Pn}(\mathbf{x}) L_{k,j}^{Pm}(\mathbf{x}) dV. \tag{23}$$

Here, $L_{i,j}^{Pn}(\mathbf{x})$ are the n-th order Lagrange polynomial for the solution point $\mathbf{x}_i$ on the cell T_j for *Pn* approximation. Using this L^2 projection procedure, $\tilde{q}_{i,j}^{h,Pm}$ is obtained and the hierarchical MLP is implemented as follows. After checking the MLP troubled-cell marker for *Pn* approximation, the projection operator to *Pm* space is defined as follows.

$$\Pi^m q_j^{h,Pn}(x) = \sum_l \tilde{q}_{l,j}^{h,Pm} L_{l,j}^{Pm}(\mathbf{x}). \tag{24}$$

3. NUMERICAL RESULTS

Extensive numerical experiments are carried out to assess the performance of the hierarchical MLP for the DG and CPR methods. Some well-known test problems on 2-D triangular and 3-D tetrahedral grids are examined up to the *P3* accuracy. As a numerical flux, RoeM (Kim 2003) scheme and AUSMPW+ (Kim 2001) scheme are adopted.

3.1 Convergence Study

Numerical accuracy in multi-dimensional inviscid compressible flows without shock wave is examined. The initial condition is set to be $(\rho_0, u_0, v_0, w_0, p_0) = (1+0.2\sin(\pi(x+y+z)), 0.5, 0.3, 0.2, 1)$, and the exact solution of density is $1+0.2\sin(\pi(x+y+z-t))$. The computational domain is $[0,2]\times[0,2]\times[0,2]$, and a periodic boundary condition is applied. Tetrahedral meshes are generated by Gmsh software (Geuzaine 2009). The error between a numerical solution and the exact solution is measured by L^p error with $p=\infty$, 1 and 2 norm. For $p \geq 1$,

$$L^p \text{ error} = \frac{1}{\sum_j |T_j|} \left\{ \sum_j \left(|T_j| \sum_i^{ndof} \left| q_j^h(\mathbf{x}_i) - q_{\text{exact}}(\mathbf{x}_i) \right|^p \right) \right\}^{1/p}, \tag{25}$$

where $|T_j|$ is the area of cell T_j. L^∞ error is computed using the maximum difference among the solution points. Table 1 shows the result of grid refinement test on tetrahedral grids. While the error of DG is smaller than that of CPR, both methods with MLP maintains the formal order-of-accuracy in smooth region.

Table 1: Grid refinement test for Euler equations on irregular grids at $t=0.25$.

	DOF	L^2	Order	CPU Time
DG-P2	10368x10	3.1261E-04	-	11.908369
	24576x10	1.2678E-04	3.14	35.902534
	48000x10	6.5227E-05	2.98	88.090376
	82944x10	3.7780E-05	3.01	183.584061
	196608x10	1.5875E-05	3.00	569.611446
DG-P3	10368x20	2.3075E-05	-	52.193214
	24576x20	7.1225E-06	4.09	161.625897
	48000x20	2.9425E-06	3.96	403.676706
	82944x20	1.4046E-06	4.06	846.423544
	196608x20	4.4356E-07	4.01	2627.760445
CPR-P2	10368x10	1.5848E-03	-	8.663248
	24576x10	6.1598E-04	3.28	27.033716
	48000x10	3.1822E-04	2.96	63.020937
	82944x10	1.9257E-04	2.75	129.660023
	196608x10	7.9686E-05	3.07	392.252533
CPR-P3	10368x20	1.2068E-04	-	29.494923
	24576x20	3.5364E-05	4.27	91.234174
	48000x20	1.5969E-05	3.56	226.003312
	82944x20	7.1925E-06	4.37	474.947794
	196608x20	2.2515E-06	4.04	1426.850471

3.2 Double Mach Reflection

This is one of the most well-known test cases for high-resolution schemes. (Woodward 1984) With the computational domain of a tube with a 30 degree ramp, a strong moving shock with $M_s = 10$ impinges on the ramp. The RoeM scheme is used as the numerical flux, and computation is carried out until $t = 0.2$.

Figure 2 shows the density contours of the DG and CPR methods on triangular grids ($h = 1/100$). The proposed limiting methods successfully provide monotonic solutions. The higher-order DG and CPR with MLP methods can significantly improve the resolution of the sheer layer and the vortex which is developed from the shock triple point and the Mach stem. It is also noted that the *P1*-projected MLP condition turns out to be more accurate in capturing detail flow structure.

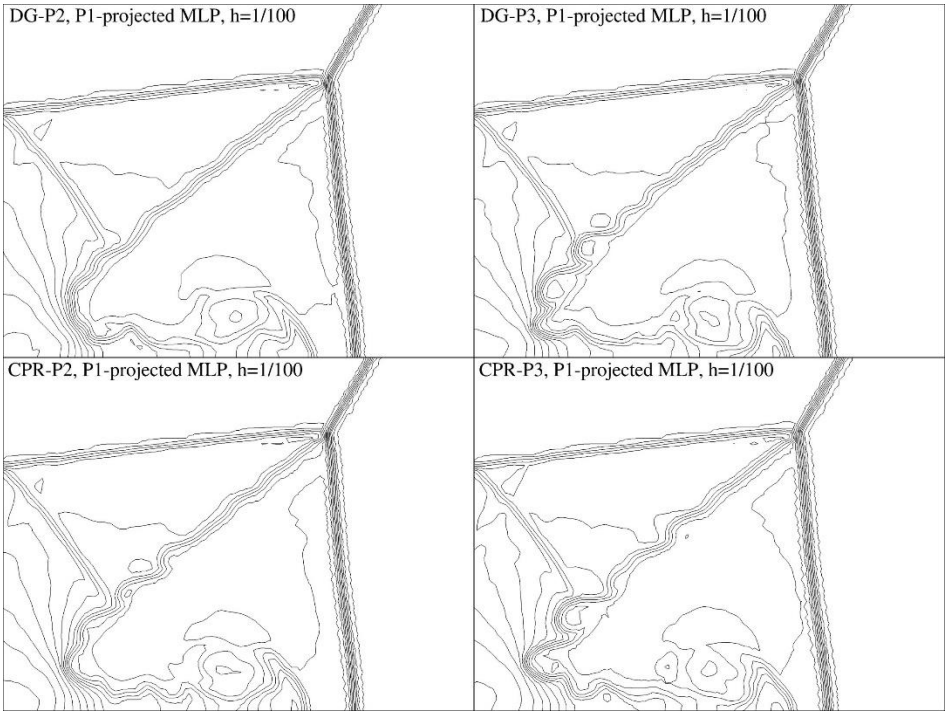

Figure 2: Comparison of density contours around the double Mach stem

3.3 Oblique Shock Mixing Layer Interaction

This test is carried out to examine the resolution of small scale vortical structures interacting with a shock discontinuity. (Yee 1999) A spatially developing compressible mixing layer produces a series of vortices, and the oblique shock originating from the upper-left corner impinges on the mixing layer. The oblique shock is deflected by the shear layer and then reflects again from the bottom slip wall, leading to the interaction between downstream vortices and the reflected shock.

As the initial condition, a hyperbolic tangent velocity profile and a convective Mach number are imposed.

$$u = 2.5 + 0.5\tanh(2y), \tag{26}$$

$$M_c = \frac{u_1 - u_2}{c_1 - c_2} = 0.6 \tag{27}$$

An oblique shock with a shock-angle of $\beta = 12°$ is imposed on the upper boundary, and a slip wall condition is applied to the lower boundary. Periodic boundary condition is applied for both ends of z-surfaces. Fluctuation adding to the mean in-flow is given by

$$v' = \sum_{k=1}^{2} a_k \cos(2\pi k\, t/T + z/L_z + \phi_k) \exp(-y^2/b), \tag{28}$$

with a period $T = \lambda/u_c$, a wavelength $\lambda = 30$ and a convective velocity $u_c = 2.68$. The other parameters are as follows: $a_1 = a_2 = 0.05$, $\phi_1 = 0$, $\phi_2 = \pi/2$ and $b = 10$. L_z, the extrusion length, is 40. The Reynolds number and the Prandtl number are 500 and 0.72, respectively. The computational domain is $[0, 200] \times [-20, 20] \times [-20, 20]$. Grid system consists of 3.5 million tetrahedral elements. With Tachyon 2 supercomputer at KISTI, MPI parallel computation was performed with 512 CPUs to reach at $t = 120$. For a better resolution, many filter methods have computed this problem on meshes clustered along the *y*-direction, but the present computation employs uniformly distributed triangular grids of $h = 0.75$.

Figure 3 shows the density contour and iso-surfaces at $t = 120$. Due to the three-dimensional perturbation (Eq. (28)), phase difference is induced along the *z*-direction. Before the oblique shock strikes the mixing layer, spanwise vortical structure is regularly developed along the *z*-direction, and after the first oblique shock-mixing layer interaction, spanwise vortical structure is noticeably deformed. After the reflected shock hits the mixing layer again, spanwise shock-vortex interaction is further developed. Higher-order approximation/reconstruction with MLP maintains the vortical structure along the downstream field.

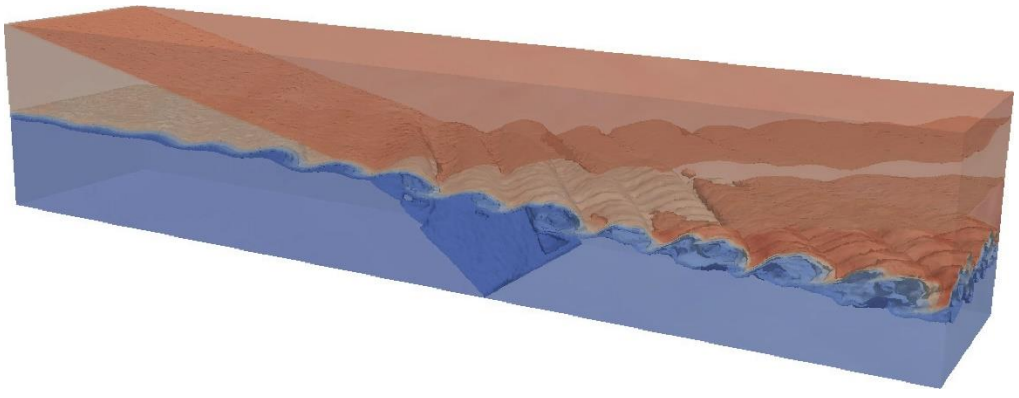

Figure 3: Density contours of three dimensional oblique shock-mixing layer interaction at $t = 120$.

4. ISSUES FOR FURTHER IMPROVEMENTS

Extensive numerical experiments validate the robustness and accuracy of the hierarchical MLP with higher-order methods in compressible inviscid and viscous flow simulations. At the same time, there are further rooms to improve and extend this limiting philosophy to deal with high-Reynolds number compressible flows around realistic configurations. Several issues are selected for discussion as follows:

4.1 Sub-cell Resolution across Shock Waves

As other limiter-based approaches, MLP enforces the monotonicity of cell-averaged values only. Thus, it may not completely control the sub-cell resolution around a shock wave. As observed in previous researches (Park submitted), current hierarchical MLP yields slight overshoots in the sub-cell distribution of a numerical shock. This may grow as a potential source of numerical instability if the order-of-accuracy is further increased, because the MLP condition is only imposed on the averaged value of the cell in which there are many degrees of freedom. Recently, there are some studies combining *hp*-refinement and limiters (Dumbser 2014). This approach requires both higher-order DG/CPR and FVM solvers, and computational overheads may become serious while switching between these solvers. Unlike limiters, artificial viscosity-based approaches does not seem to suffer from this issue. Instead, there are tuning parameters to determine the diffusion, which usually relies on the flow structure, grid system and the desired order-of-accuracy (Persson 2006). Despite some progresses to determine such tuning parameters, it appears that artificial viscosity is not robust enough yet to resolve very strong shock and expansion waves (Yu 2014, Park 2014 (ICCFD)). In the context of MLP concept, more research efforts needs to be directed to this issue by controlling the limited approximation or reconstruction.

4.2 Convergence for Steady Flow Problems

Up to now, the hierarchical MLP has been developed mainly for unsteady flow problems. While its performances are validated, convergence issue for steady-state problems still remains. It is well-known that slope limiters whose operations are non-differentiable, may fail to reach a convergent solution even in finite volume methods. Such non-differentiable operators are sensitive to the numerical fluctuations near shock wave and they may become stalled. While we proposed the MLP-u2 slope limiters to overcome this issue (Park 2010, Park 2012), the troubled-cell detecting mechanism and projection operator for the DG and CPR methods are still non-differentiable. In addition, higher-order CFD methods have a reduced damping mechanism for transient error, thus this situation may become more problematic. Implicit time integrations are preferred to compute steady flow problems, but it is quite untractable to construct an implicit operator for non-differentiable hierarchical MLP. It appears that additional smooth transition mechanism between troubled-cell and normal-cell is necessary.

4.3 Interaction of Turbulent Vortices with Shock Waves

One of the promising areas for higher-order methods is turbulent flows. Especially, researchers expect higher-order schemes to accurately resolve interactions between

shock and turbulent vortices around high-speed vehicles. Recent researches attempt to calculate turbulence by Reynolds-averaged Navier-Stokes (RANS) equations with Spalart-Allmaras model (Nguyen 2007) and $k-\omega$ model (Bassi 2005), and by DNS/LES approaches (Wang 2013). Numerical experiments reveal that current higher-order CFD methods are not robust as finite volume RANS solvers, primarily due to the nonsmoothness introduced in turbulence models (Wang 2013). Recently, there are some progresses to improve the accuracy of turbulence models by modifying closure models (Nguyen 2007, Allmaras 2012), by developing hybrid RANS-LES models (Spalart 1997, Spalart 2006), or by introducing transition models (Langtry 2009). The enhanced resolution of higher-order methods makes it possible to accurately simulate highly unsteady turbulent flow and/or laminar-turbulent transitions with improved turbulence and/or transition models. However, there are few studies to simulate turbulent flows with shock waves with higher-order methods. Since excessive numerical viscosity of shock-capturing schemes may easily dissipate small scale vortical structure, accurate shock-capturing schemes are indeed essential. From successful numerical experiments, we are expecting that the hierarchical MLP limiting may provide a proper dissipation-control mechanism to capture detailed turbulent flows as well as shock waves.

5. CONCLUSIONS

Guided by the MLP condition and the maximum principle, the hierarchical MLP limiting is successfully extended into the higher-order CFD methods such as the DG and CPR methods. The extended forms of the MLP condition, *i.e.*, the augmented MLP condition and the $P1$-projected MLP condition, are proposed to treat the solution points near discontinuities without compromising the higher-order nature in smooth region. The uncertainty of determining a parameter for slope limiting is then eliminated by examining the behavior of local extrema near vertex point. Finally, the hierarchical MLP limiting is formulated by combining one of the extended MLP conditions with the MLP extrema detector.

Extensive computations, ranging from scalar conservation laws to multi-dimensional flow systems, are carried out up to *P3* approximation to examine the capability of the hierarchical MLP methods in capturing multi-dimensional flow physics. Numerous comparisons and grid refinement tests on unstructured grids demonstrate the proposed limiting provides detailed multi-dimensional flow structures without numerical oscillations in discontinuous region, while maintaining the required accuracy in smooth region. The hierarchical MLP limiting is robust and efficient in the sense that it does not require any tuning parameter and it is applied to conservative variables without characteristic decomposition. At the same time, more efforts need to be exerted in the areas of sub-cell resolution, steady-state convergence and turbulence/transition models in order to extend the current approach to the simulations of high-Reynolds number compressible flows around realistic configurations.

ACKNOWLEDGMENTS

The author appreciates the financial supports by the EDISON program through the National Research Foundation of Korea (NRF) funded by the Ministry of Science, ICT & Future Planning (NRF-2011-0020559) and by NSL (National Space Laboratory) program through the National Research Foundation of Korea funded by the Ministry of Education, Science and Technology (NRF-2014M1A3A3A02034856). This work is also partially supported by the RoK ST&R project of Lockheed Martin Corporation. The author also appreciates the computing resources provided by the KISTI Supercomputing Center (KSC-2014-C3-054) and Kwangseok Oh's help in preparation of this manuscript.

REFERENCES

Allmaras, S. R., Johnson, F. T., and Spalart, P. R. (2012), "Modifications and Clarifications for the Implementation of the Spalart-Allmaras Turbulence Model," *ICCFD7-1902.*

Bassi, F., Crivellini, A., Rebay, S., and Savini, M. (2005), "Discontinuous Galerkin solution of the Reynolds-averaged Navier-Stokes and k-w turbulence model equations," C & F, **34**(4-5), 507–540.

Castonguay, P., Vincent, P. E., and Jameson, A. (2011), "A new class of high-order energy stable flux reconstruction schemes for triangular elements," J Sci Comput, **51**(1), 224–256.

Cockburn, B. and Shu, C.-W. (1998), "The Runge-Kutta discontinuous Galerkin method for conservation laws V: multidimensional systems," J Comput Phys, **141**, 199–224.

Cockburn, B., Karniadakis, G. E., and Shu, C.-W. (2000), "Discontinuous Galerkin Methods: Theory, Computation and Applications," Springer-Verlag Inc., Berlin, Germany.

Dumbser, M., Zanotti, O., Loubere, R., and Diot, S. (2014), "A posteriori subcell limiting of the discontinuous Galerkin finite element method for hyperbolic conservation laws," J Comput Phys, **278**, 47–75.

Geuzaine, C. and Remacle, J.-F. (2009), "Gmsh: A 3-D finite element mesh generator with built-in pre- and post-processing facilities," Int J Num Methods Eng, **79**(11), 1309–1331.

Huynh, H. T. (2007), "A flux reconstruction approach to high-order schemes including discontinuous Galerkin methods," *18th AIAA Computational Fluid Dynamics Conference*, Miami.

Huynh, H. T. (2009), "A reconstruction approach to high-order schemes including discontinuous Galerkin for diffusion," *47th AIAA Aerospace Sciences Meeting Including The New Horizons Forum and Aerospace Exposition*, Orlando.

Kim, K. H., Kim, C., and Rho, O.-H. (2001), "Methods for the accurate computations of hypersonic flows I.AUSMPW+ scheme," J Comput Phys, **174**(1), 38–80.

Kim, K. H. and Kim, C. (2005), "Accurate, efficient and monotonic numerical methods for multi-dimensional compressible flows: Part II: Multi-dimensional limiting process," J Comput Phys, **208**(2), 570–615.

Kim, S.-s., Kim, C., Rho, O.-H., Kyu Hong, S., and Hong, S. K. (2003), "Cures for the shock instability: Development of a shock-stable Roe scheme," J Comput Phys, **185**(2), 342–374.

Krivodonova, L., Xin, J., Remacle, J.-F., Chevaugeon, N., and Flaherty, J. E. (2004), "Shock detection and limiting with discontinuous Galerkin methods for hyperbolic conservation laws," Appl Num Math, **48**(3-4), 323–338.

Langtry, R. B. and Menter, F. R. (2009), "Correlation-based transition modeling for unstructured parallelized computational fluid dynamics codes," AIAA journal, **47**(12), 2894–2906.

Nguyen, N. C., Persson, P.-O., and Peraire, J. (2007), "RANS solutions using high order discontinuous Galerkin methods," *45th AIAA Aerospace Sciences Meeting and Exhibit*, Reno.

Park, J. S., Yoon, S.-H., and Kim, C. (2010), "Multi-dimensional limiting process for hyperbolic conservation laws on unstructured grids," J Comput Phys, **229**(3), 788–812.

Park, J. S. and Kim, C. (2012), "Multi-dimensional limiting process for finite volume methods on unstructured grids," C & F, **65**, 8–24.

Park, J. S. and Kim, C. (2014), "Higher-order multi-dimensional limiting strategy for discontinuous Galerkin methods in compressible inviscid and viscous flows," C & F, **96**, 377–396.

Park, J. S., Yu, M., Kim, C., and Wang, Z. J. (2014), "Comparative Study of Shock-Capturing Methods for High-Order CPR: MLP and Artificial Viscosity," *ICCFD8 2014-0067*.

Park, J. S. and Kim, C. (submitted), "Hierarchical multi-dimensional limiting strategy for correction procedure via reconstruction," J Comput Phys.

Persson, P.-o. and Peraire, J. (2006), "Sub-cell shock capturing for discontinuous Galerkin methods," *44th AIAA Aerospace Sciences Meeting and Exhibit*, Reno.

Spalart, P., Jou, W., Strelets, M., and Allmaras, S. (1997), "Comments on the feasibility of LES for wings, and on a hybrid RANS/LES approach," Advances in DNS/LES, **1**, 4–8.

Spalart, P. R., Deck, S., Shur, M., Squires, K., Strelets, M. K., and Travin, A. (2006), "A new version of detached-eddy simulation, resistant to ambiguous grid densities," Theo Comput fluid dyn, **20**(3), 181–195.

Vincent, P. E. and Jameson, A. (2011), "Facilitating the adoption of unstructured high-order methods amongst a wider community of fluid dynamicists," Mathematical Modelling of Natural Phenomena, **6**(3), 97–140.

Vincent, P. E., Castonguay, P., and Jameson, A. (2011), "A new class of high-order energy stable flux reconstruction schemes," J Sci Comput, **47**(1), 50–72.

Wang, Z. J. (2007), "High-order methods for the Euler and Navier-Stokes equations on unstructured grids," Progress in Aerospace Sciences, **43**(1-3), 1–41.

Wang, Z. J. and Gao, H. (2009), "A unifying lifting collocation penalty formulation including the discontinuous Galerkin, spectral volume/difference methods for conservation laws on mixed grids," J Comput Phys, **228**(21), 8161–8186.

Wang, Z. J. (2011), "Adaptive High-Order Methods in Computational Fluid Dynamics," **2**, World Scientific Publishing Inc., Singapore.

Wang, Z. J., Fidkowski, K., Abgrall, R., Bassi, F., Caraeni, D., Cary, A., Deconinck, H. *et al.* (2013), "High-order CFD methods: current status and perspective," Int J Num Methods Fluids, **72**(8), 811–845.

Woodward, P. R. and Colella, P. (1984), "The numerical simulation of two-dimensional fluid flow with strong shocks," J Comput Phys, **54**(1), 115–173.

Yee, H. C., Sandham, N. D., and Djomehri, M. J. (1999), "Low-dissipative high-order shock-capturing methods using characteristic-based filters," J Comput Phys, **150**(1), 199–238.

Yoon, S.-H., Kim, C., and Kim, K.-H. (2008), "Multi-dimensional limiting process for three-dimensional flow physics analyses," J Comput Phys, **227**(12), 6001–6043.

Yu, M. and Wang, Z. J. (2014), "Shock capturing for the Correction Procedure via Reconstruction method using artificial viscosity and diffusivity," *ICCFD8 2014-0079*.